Polymer 226 (2021) 123812

Contents lists available at ScienceDirect

Polymer

journal homepage: www.elsevier.com/locate/polymer

Nanostructural organization of thin films prepared by sequential dip-coating deposition of poly(butylene succinate), poly(ε-caprolactone) and their copolyesters (PBS-*ran*-PCL)

Mario Iván Peñas [a,b], Connie Ocando [b], Evis Penott-Chang [c], Maryam Safari [b], Tiberio A. Ezquerra [d], Esther Rebollar [e], Aurora Nogales [d], Rebeca Hernández [a,*], Alejandro J. Müller [b,c,f,**]

[a] Instituto de Ciencia y Tecnología de Polímeros, ICTP-CSIC, Juan de la Cierva, 3, 28006, Madrid, Spain
[b] POLYMAT y Departamento de Polímeros y Materiales Avanzados: Física, Química y Tecnología, Facultad de Química, Universidad del País Vasco UPV/EHU, Paseo Manuel de Lardizabal 3, 20018, Donostia-San Sebastián, Spain
[c] Grupo de Polímeros I USB, Departamento de Ciencias de los Materiales, Universidad Simón Bolívar, 1080A, Caracas, Venezuela
[d] Instituto de Estructura de la Materia, IEM-CSIC, Serrano 121, 28006, Madrid, Spain
[e] Instituto de Química Física Rocasolano, IQFR-CSIC, Serrano 119, 28006, Madrid, Spain
[f] IKERBASQUE, Basque Foundation for Science, Bilbao, Spain

ARTICLE INFO

Keywords:
Poly(ε-caprolactone)
poly(butylene succinate)
Random copolyesters
Thin-films
Layer-by-layer dip-coating
s-SNOM
nano-FTIR

ABSTRACT

In this work, we prepare and characterize multiphasic thin films containing poly(ε-caprolactone), PCL, poly (butylene succinate), PBS, and a poly (butylene succinate-*ran*-ε-caprolactone) (PBS-*ran*-PCL) random copolyester. To that aim, thin films were prepared by sequential dipping of a silicon substrate into chloroform solutions of the respective polymers. The preparation method resulted in films with varying compositions of PCL and PBS components depending on the initial concentration of the dipping solutions and the number of dipping steps employed for the preparation of the samples. Atomic force microscopy (AFM), grazing incidence X-ray scattering at wide angle (GIWAXS) and scattering-type scanning near-field optical microscopy (s-SNOM) and Fourier transform infrared nanospectroscopy (nano-FTIR) were employed to characterize the films obtained. As chloroform can dissolve all components, the final composition of the film was always rich in the last deposited layer component. The thin films obtained were semicrystalline with a complex axialitic or dendritic morphology of the dominant component (that one deposited last) with traces of the other components, whose presence and location was revealed by s-SNOM/nano-FTIR.

1. Introduction

Poly(ε-caprolactone) (PCL) and poly(butylene succinate) (PBS) are fully biodegradable aliphatic polyesters. They have attracted a great deal of attention for the development of biodegradable packaging and biomedical applications, such as implant devices, tissue scaffolds and wound dressings [1]. The blending of biodegradable polyesters is considered one of the most promising ways to obtain sustainable materials with enhanced and tailored properties. PCL/PBS blends have been prepared by melt blending or solution mixing methods attempting to improve the properties of the individual polymers. Regardless of the preparation method used, PCL/PBS blends are immiscible, as evidenced by composition independent T_gs and a biphasic melt, which leads to poor interfacial adhesion and macrophase separation [2]. Nevertheless, earlier reports on PBS/PCL blends have indicated that a noticeable improvement in the mechanical properties of PBS/PCL blends could be obtained. These results were explained by considering possible interactions between the ester groups of the neat polymers through hydrogen bonds [3]. Although bulk properties of these two polymers and their blends have been extensively studied [4] [–] [7], not much

* Corresponding author. Instituto de Ciencia y Tecnología de Polímeros, ICTP-CSIC, Juan de la Cierva, 3, 28006, Madrid, Spain.
** Corresponding author. POLYMAT y Departamento de Polímeros y Materiales Avanzados: Física, Química y Tecnología, Facultad de Química, Universidad del País Vasco UPV/EHU, Paseo Manuel de Lardizabal 3, 20018, Donostia-San Sebastián, Spain.
E-mail addresses: rhernandez@ictp.csic.es (R. Hernández), alejandrojesus.muller@ehu.es (A.J. Müller).

https://doi.org/10.1016/j.polymer.2021.123812
Received 30 January 2021; Received in revised form 19 April 2021; Accepted 21 April 2021
Available online 5 May 2021

information about the structure and morphology of their thin and ultrathin films has been reported.

Thin polymer films obtained from deposition of polymer blends in solution has been widely reported in literature as a bottom up method to produce patterned surfaces arising from different phenomena such as dewetting and phase separation [8]. The preparation of thin polymer films through sequential deposition of polymer aqueous solutions, known as layer-by-layer (LbL) method has been widely investigated to achieve nanostructured films and coatings through the incorporation of successive polymer layers that interact with each other electrostatically, H-bonded or covalently [9] [–] [11]. In contrast, the preparation of thin polymer films through sequential deposition of different polymers in organic solutions is less addressed in literature. Such method of preparation allows to deposit first a polymer layer on a substrate to have an ordered structure followed by the deposition of a second layer of a different polymer (or organic molecule) in order to minimize their intermixing. Such approach has been employed mostly for the preparation of thin films applied as electronic devices and energy conversion set-ups [12] [–] [14].

The morphology of polymer thin films deposited by spin-coating is mostly driven by the composition of the polymer solution and post-treatments such as thermal or solvent annealing are employed as a mean to modulate their final morphology. During the annealing process, surface segregation is induced by preferential wetting of one component in polymer blends and block copolymer thin films [15]. This phenomenon known as surface wetting induced surface segregation results in changes of the surface chemical composition of thin films and influences crystallization for crystalline block copolymer thin films and blends [16] [–] [19]. On the other hand, for thin films obtained by dip-coating, the final film morphology depends to a high extent on the experimental conditions, such as withdrawal speed, nature of the solvent, solution concentration and geometry of the reservoir and it can be modulated without the need of additional post annealing techniques [20–22]. Within this context, dip-coating constitutes one effective process for the fabrication of thin polymer films, with extensive application in small-scale fabrication for academic studies [23]. The method is based on the deposition of thin films via precision immersion and withdrawal of a substrate into a reservoir containing a polymer solution. Specifically, dip-coating has been extensively reported to prepare PCL thin films that can be employed as coatings for degradation prevention in biodegradable magnesium alloys and blend coatings with PEG for their application as biomaterials [24,25]. To the best of our knowledge, the preparation and characterization of PCL/PBS thin polymer films have not been described in the literature.

In this study, thin films of PCL, PBS and a random copolyester (PBS-*ran*-PCL) were prepared by sequential dipping steps of a silicon substrate into chloroform solutions of the respective polymers, previously synthesized by some of us [26]. The use of poly (butylene succinate-*ran*-ϵ-caprolactone) (PBS-*ran*-PCL) copolymer layers together with PCL and/or PBS is expected to improve miscibility, interfacial adhesion and the resultant mechanical properties of PCL/PBS blends as previously reported [27]. A nearly symmetric copolymer was chosen for this study, as this has a better chance of interacting with neat PCL and neat PBS, hence it would have a better chance to promote adhesion between a layer of neat PBS and a layer of neat PCL. Copolymer compositions different to approximately 50/50 would be more compatible with either PBS or PCL depending on the composition. The resulting morphology was observed by atomic force microscopy (AFM), and it was related to the thickness and composition of the films. The presence of PCL or PBS crystals was explored by grazing incidence X-ray scattering at wide angle (GIWAXS). Previous studies carried out on blend thin films prepared by dip-coating have employed selective dissolution of one of the polymers in order to be able to assign the polymer phases observed in AFM images [22]. For the films under study here, it is not possible to selectively eliminate one polymer as the three polymers dissolve in common solvents. Therefore, scattering-type scanning near-field optical microscopy (s-SNOM) and Fourier transform infrared nanospectroscopy (nano-FTIR) were employed in selected samples to image the local distribution of the three polymers in the films under study. The information obtained allows us to correlate the dip-coating processing employed for the preparation of the samples to the structure and morphology exhibited by PCL/PBS thin films.

Table 1
Molecular characterization data[a].

Polymer	Composition (BS/CL mol/mol)	M_w (g/mol)	M_w/M_n
PBS	(100/0)	21,470	2.9
PCL	(0/100)	17,400	3.2
COPOL	(51/49)	23,500	3.1

[a] Data taken from Ref. [26].

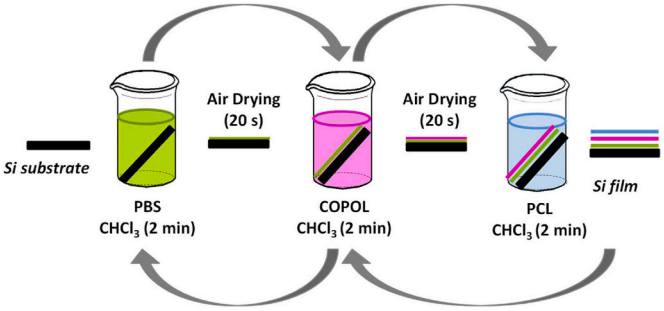

Scheme 1. Schematic representation of the method of preparation of the films.

2. Experimental part

2.1. Materials

Poly (butylene succinate) (PBS), poly (ϵ-caprolactone) (PCL) and a poly (butylene succinate-*ran*-ϵ-caprolactone) random copolyester, designated as COPOL, were synthesized according to a method reported elsewhere [26]. Table 1 reports the average molecular weight and composition for the polymers under study.

2.2. Thin films preparation

Solutions of PCL, PBS and COPOL were prepared by dissolving the appropriate mass of polymer in $CHCl_3$ to obtain concentrations of 1 mg/mL and 2 mg/mL. Thin films of PCL, PBS, and COPOL were prepared by dip-coating silicon wafers ($40 \times 9 \times 0.5$ mm^3), previously washed out from impurities with a piranha solution (60:40 H_2SO_4:H_2O_2), into the corresponding $CHCl_3$ solutions during 2 min. The film drying time for pristine thin films of PCL, PBS, and COPOL was determined by visualization of the height position of the drying line after withdrawing sample, located by a sharp colour (see supplementary video). The evaporation speed, calculated by considering that the solution height was maintained at 30 mm, was ~3 mm s^{-1} in all cases. It is important to note that concentrations of the polymers in the dipping solutions higher than 2 mg/mL led to the formation of stripes on the surface of the film, perpendicularly to the withdrawal direction (see Figure S1, in the Supplementary Information). This phenomenon, named "stick-slip motion" has been observed and described for films prepared by dip-coating, and it is the result of the deposition of high concentrations of the polymer in the upper part of the meniscus giving rise to the formation of local thickness heterogeneities [22].

For the preparation of films containing PBS, PCL, and COPOL, Si wafers were sequentially immersed in $CHCl_3$ solutions of PCL, COPOL, and PBS at 1 and 2 mg/mL (series I and II, respectively). A schematic representation of the process employed for the preparation of the

samples is shown in Scheme 1. The immersion time was 2 min with an air-drying step of 20 s in between dipping steps.

Films corresponding to series I were 3-layer films prepared from $CHCl_3$ solutions of PCL, COPOL, and PBS at 1 mg/mL. The difference among them was the order employed for the deposition of the polymers. For the film designated as 3-layer (PBS)_1, the last deposited layer was PBS (i.e., the layers were deposited in the following order: PCL, COPOL and PBS), and for the film designated as 3-layer (PCL)_1, the last deposited layer was PCL (i.e., the layers were deposited in the following order: PBS, COPOL and PCL).

Films corresponding to series II were prepared from $CHCl_3$ solutions of PCL, COPOL, and PBS at 2 mg/mL. Two films were prepared with different number of layers (3 and 13) in order to determine the effect of the number of layers on the morphology of the resulting films. In both cases, the last deposited layer was PBS. The 3-layer film was designated as 3-layer (PBS)_2, whereas the 13-layer film was designated as 13-layer (PBS)_2.

2.3. Nuclear magnetic resonance (NMR)

Thin polymer films were dissolved in 1 mL of deuterated chloroform and ^{1}H NMR spectra were taken in a Varian System 500 MHz NMR equipment.

2.4. Atomic force microscopy (AFM)

The morphology and thickness of the layers were observed by AFM (Multimode Scanning Probe Microscope, Veeco/Bruker), employing a di NanoScope IVa Controller with the conventional height mode (tapping mode, normal AFM) at a nominal force constant of 42 N/m and 320 kHz resonant frequency. The AFM samples ($9 \times 9 \times 0.5$ mm^3) were cut from the previously prepared films on silicon wafer substrates. Film thicknesses were measured by AFM by the scratch method and the results were compared to those obtained from the analysis of the AFM height profiles. WSxM5.0 software was employed for the visualization and analysis of the AFM images.

2.5. X-ray scattering

Grazing incidence X-ray scattering at wide angle (GIWAXS) was measured using synchrotron radiation at the NCD-SWEET beamline at the ALBA Synchrotron (Cerdanyola del Vallès, Barcelona, Spain). The sample was inclined to achieve different incidence angles, ranging from 0.1° to 0.3° between the sample surface and the X-ray beam. The X-ray wavelength used was 1 Å. The scattering intensity was collected by a Rayonix detector of 960 × 2880 pixels (pixel size 88.54 μm), placed at 145.6 mm from the sample. Patterns acquired with an exposition time of 5 s were corrected for background scattering and analyzed by the Fit2D software [28].

2.6. Scattering-type scanning near-field optical microscopy (s-SNOM) and fourier transform infrared nanospectroscopy (nano-FTIR)

s-SNOM, based on the AFM technique, is carried out with a metallized tip which is illuminated with a monochromatic infrared laser radiation concentrated at the vertex of the tip, acting as an antenna. s-SNOM yields infrared amplitude and phase infrared images at nanoscale resolution and allows to obtain maps of the chemical properties of the surface of the sample. Nano-FTIR is based on s-SNOM, where the tip is illuminated with a broadband infrared radiation. The tip-scattered light is recorded with an asymmetric Fourier transform spectrometer at a fixed sample position, yielding amplitude- and phase-resolved infrared spectra [29] [–] [31].

A commercial s-SNOM/nano-FTIR setup (NeaSNOM, Neaspec GmbH, Germany) was employed for measuring s-SNOM phase images and nano-FTIR phase spectra using gold-coated commercial Si tips (Nanosensors, PPP-NCSTAu) with a mechanical resonance frequency ~135 kHz for tapping mode atomic force microscope (AFM). s-SNOM imaging was collected directly on thin film samples prepared in silicon wafers by means of a microscope equipped with a MIRcat laser (MIRcat Mid-IR laser, Daylight Solutions, USA), at a laser power of 3 mW, and a tapping amplitude of 50 nm. The acquisition time of one s-SNOM image was 11 min. For nano-FTIR, a broadband infrared laser continuum was employed with an average output power of ~600 μW covering a spectral range from 2200 to 650 cm^{-1}. All nano-FTIR spectra were recorded with a spectral resolution of 17 cm^{-1} and a tapping amplitude of 80 nm. Reported nano-FTIR spectra are averages of 10 full spectra.

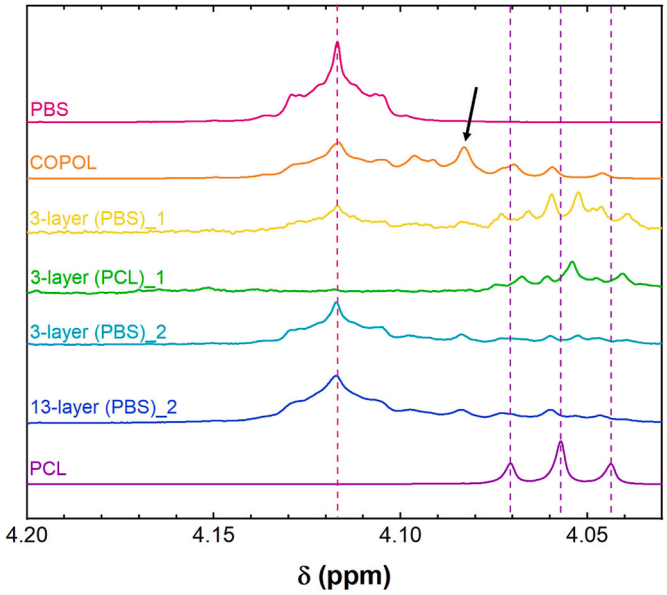

Fig. 1. ^{1}H NMR spectra in the 4.00–4.20 ppm region of films corresponding to series I, 3-layer (PBS)_1 and 3-layer (PCL)_1, and series II, 3-layer (PBS)_2 and 13-layer (PBS)_2. For comparison, the spectra corresponding to neat PBS, PCL and COPOL are also included in the figure.

3. Results and discussion

3.1. Determination of the composition of the films

The process of sequential dip coating employed for producing the films takes place through sequential immersion of a silicon substrate onto chloroform solutions of each of the polymers as shown in Scheme 1. Given the fact that chloroform is a solvent for PCL, PBS and COPOL, as a first step, we set to determine the (BS/CL) ratio for all the samples under study. For comparison, the spectra corresponding to neat PBS, PCL and COPOL (see chemical structures in Figure S2, in the Supplementary Information) are also included in Fig. 1 and the peaks are assigned according to literature [26]. The triplet signal centered at 4.06 ppm can be assigned to the methylene proton resonance of CH_2 (7) in PCL and the multiplet signal centered at 4.12 ppm corresponds to the proton resonances of CH_2 (1,4) in PBS. For COPOL, it was not possible to obtain separate signals corresponding to PBS and PCL sequences within this ppm region. In the films, the presence of a resonance peak at 4.08 ppm that can be assigned to COPOL (marked with an arrow in Fig. 1) is observed, most notably for films corresponding to series II, which confirms the presence of the three components for all the samples under study. Nevertheless, a quantitative determination is not possible due to the overlapping of the NMR signals of the COPOL with those corresponding to the pristine polymers, PBS and PCL.

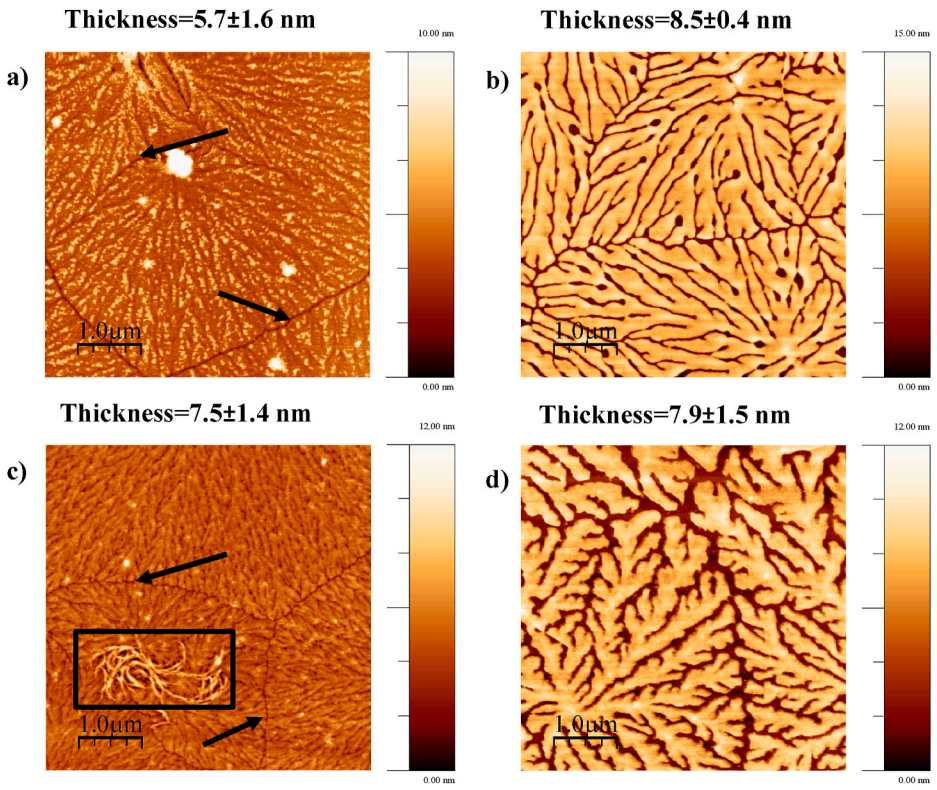

Fig. 2. Tapping mode AFM height images of **a)** PBS films, **b)** PCL films **c)** 3-layer (PBS)_1 and **d)** 3-layer (PCL)_1 prepared by dip-coating from $CHCl_3$ solutions at 1 mg/mL. Black arrows mark the straight boundaries observed between superstructural structures (spherulites, axialites or dendrites) which are caused by the impinging of these structures as they grow radially. The black square in Fig. 2c marks the occurrence of new crystalline morphologies as explained in the text.

Table 2
Nomenclature employed for all the samples under study.

Sample	C (mg/mL)[a]	Number of layers	Last deposited layer
Series I			
3-layer (PBS)_1	1	3	PBS
3-layer (PCL)_1	1	3	PCL
Series II			
3-layer (PBS)_2	2	3	PBS
13-layer (PBS)_2	2	13	PBS

[a] Concentration of the dipping solutions.

3.2. Study of the morphology and crystallinity

Fig. 2 shows AFM height images for pristine films obtained from $CHCl_3$ solutions of PBS and PCL and films corresponding to series I prepared at polymer concentrations of 1 mg/mL, 3-layer (PBS)_1 and 3-layer (PCL)_1. All the samples under study are ultrathin films with thicknesses below 10 nm as determined by AFM by the scratch method. The results were shown to match the depth profile analyzed for each of the samples, both analysis are shown in the supplementary information (Figure S3, in the Supplementary Information).

The morphology of PCL in ultra-thin films has been reported in the literature [32,33], however, to the best of our knowledge, there are no studies regarding the morphology of PBS in ultra-thin films. Films obtained from $CHCl_3$ solutions of PBS at 1 mg/mL (Fig. 2a) exhibit a semi-crystalline morphology rich in edge-on lamellae radiating from central nuclei that resemble spherulitic/axialitic superstructures, whereas the morphology exhibited by PCL thin films is dendritic (Fig. 2b). In all cases, the relatively straight boundaries between superstructural structures (spherulites, axialites or dendrites), which are caused by the impinging of these structures as they grow radially, can be clearly observed in Fig. 2. The morphology observed in Fig. 2b for PCL (thickness~8 nm) is consistent with that reported for spin-coated PCL films from PCL-toluene solution for which dense-branching morphology (DBM) and dendrites were observed when $t < 2Rg$ (at thicknesses below 12 nm), related to the diffusion-limited aggregation (DLA) process [32]. The morphology corresponding to the COPOL sample consists of PBS-rich phase spherulitic/axialitic crystals (see Figure S4, in the Supplementary Information). Extensive previous studies by WAXS and DSC have shown that in this isodimorphic copolymer sample, only the PBS-rich phase can crystallize [25].

Both films of series I (3-layer films described in Table 2) have thicknesses that are comparable within the experimental error and are also similar to those of neat components single layer films, ~7.5 nm for the films of series I and 5.7 and 8.5 nm for neat PBS and PCL respectively (at 1 mg/mL). This is as a result of the partial dissolution of the films in $CHCl_3$ during the consecutive deposition steps, since chloroform dissolves both PCL and PBS. Still, the presence of the three polymers could be ascertained through ^{1}H NMR as shown in Fig. 1. In general terms, the morphology observed by AFM on the film surfaces is determined by the last deposited polymer layer which confirms the sequential deposition of the polymers onto the silicon substrate. Therefore, films that were coated with PBS as last layer show a similar spherulitic/axialitic morphology to that exhibited by neat PBS films (single layer) dip-coated from chloroform solution. Correspondingly, those in which the last applied layer was PCL display the dendritic morphology observed in neat PCL films (single layer). The morphology observed for the 3-layer (PCL)_1 sample is analogous to that reported for PS/PCL blend films with film thickness of about 15 nm, for which the crystallization of PCL leads to the formation of PCL dendritic crystals [19]. It is important to note that Fig. 2c shows the development of a new crystalline morphology with respect to the morphology observed for pristine PBS films (Fig. 2a). On top of the spherulitic structure, we observe curved structures (highlighted with a square in Fig. 2c). These curved crystals have been previously reported for PLLA ultrathin films and related to

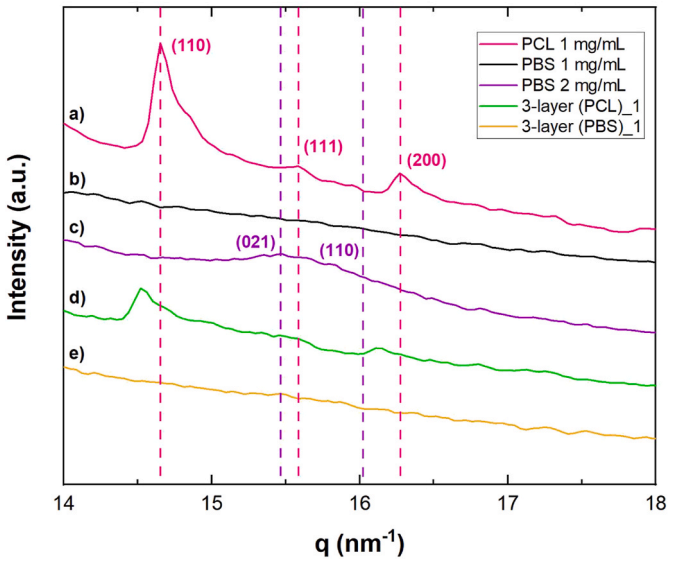

Fig. 3. Intensity as a function of the scattering vector *q* as calculated from the corresponding GIWAXS patterns (shown in the Supplementary Information, Figure S5). **a)** PCL 1 mg/mL, **b)** PBS 1 mg/mL, **c)** PBS 2 mg/mL, **d)** 3-layer (PCL)_1, **e)** 3-layer (PBS)_1.

edge-on lamellae [34,35], in very thin films (thicknesses around and below 10 nm). A study of the crystal unit cell parameters and chain orientation of thin films of linear aliphatic polyesters revealed that lamellar crystal edge-on morphology seems to be the preferred configuration for aliphatic polyesters. This is related to the establishment of a molecular interaction of the carbonyl groups of the polyesters, lying on the *bc* face parallel to the substrate plane, with the outer silicon oxide layer of the substrate that controls the chain fixation to the substrate [36].

The crystallization of the films was further investigated by Grazing Incidence X Ray Diffraction analysis and the diffractograms obtained using GIXRD at 0.1° incidence angle are shown in Fig. 3. For the pristine PCL film (1 mg/mL), with thickness as low as 8.5 nm, the characteristic diffractions of (110), (111) and (200) planes are clearly distinguished in Fig. 3a, [37]. For the pristine PBS film (1 mg/mL), the GIWAXS diffractogram in Fig. 3b showed no diffraction peaks even though a semicrystalline morphology was observed for this film in AFM images (Fig. 2a). In contrast, a broad peak at 15.5 nm^{-1} is observed for the PBS film prepared from chloroform solutions of PBS at 2 mg/mL (Fig. 3c), which is attributed to the diffraction of the (021) plane. Note that the peak corresponding to the diffraction of the (110) plane at 16.0 nm^{-1}, is also included within this broad peak [38,39].

Regarding the results obtained for blend thin films, only the 3-layer (PCL)_1 sample showed the characteristic diffraction peaks of PCL, placed as the outermost layer for this sample (Fig. 3d). For this sample, the diffraction peaks are shifted to the left with respect to the diffraction peaks observed for the pristine PCL film (Fig. 3a). This might be a result of the different spreading of crystallites on the illuminated area [40]. As shown in Fig. 2, the distribution of crystals appears to be more homogeneous in the case of the PCL film (Fig. 2b) compared to the distribution of crystals observed for sample 3-layer PCL (Fig. 2d). This might result in contributions in different positions of the diffraction centers which causes a shifting to the left of the diffraction peaks corresponding to the sample 3-layer PCL (Fig. 3d) with respect to the sample PCL (Fig. 3a). In contrast, neither the sample 3-layer (PBS)_1 (Fig. 3e) nor the samples corresponding to series II, for which the outermost layer was PBS, showed diffraction peaks in GIWAXS experiments (results not shown). This is an apparent inconsistency with the AFM results shown in Fig. 2 that clearly show an spherulitic/axialitic structure for pristine PBS films as well as for films whose last layer is PBS. In order to explain these results it is important to take into account the process of preparation of the samples through dip-coating. For this process, the evaporation rate of the solvent plays an important role on the crystallization of the polymers. Spherulite/axialite growth is the consequence of the

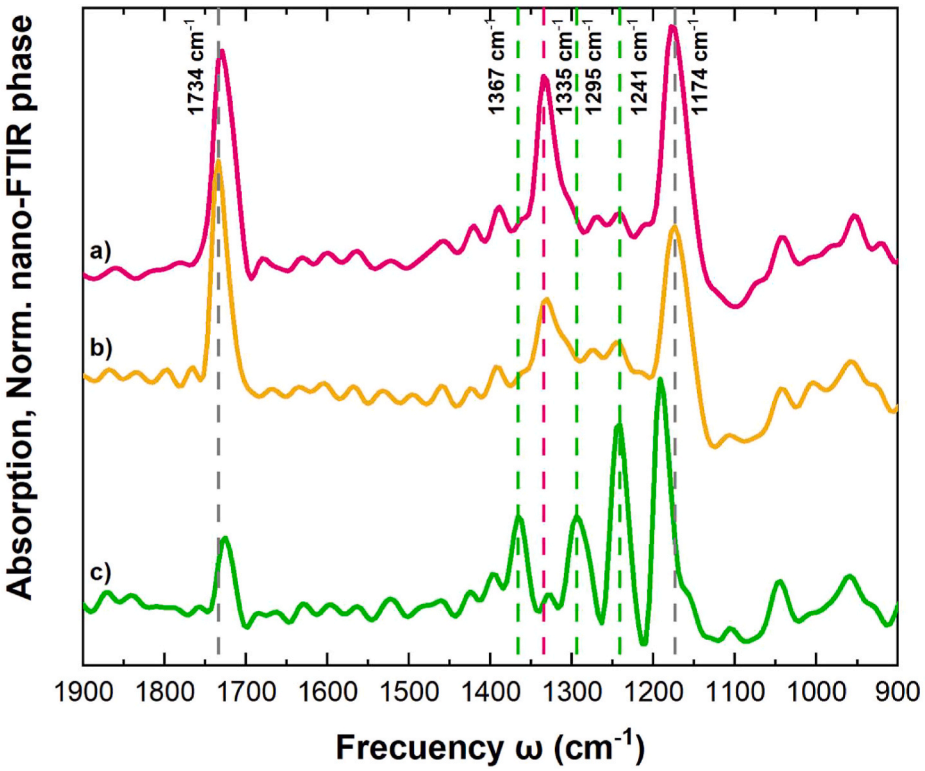

Fig. 4. Nano-FTIR spectra of pristine films of **a)** PBS, **b)** COPOL and **c)** PCL.

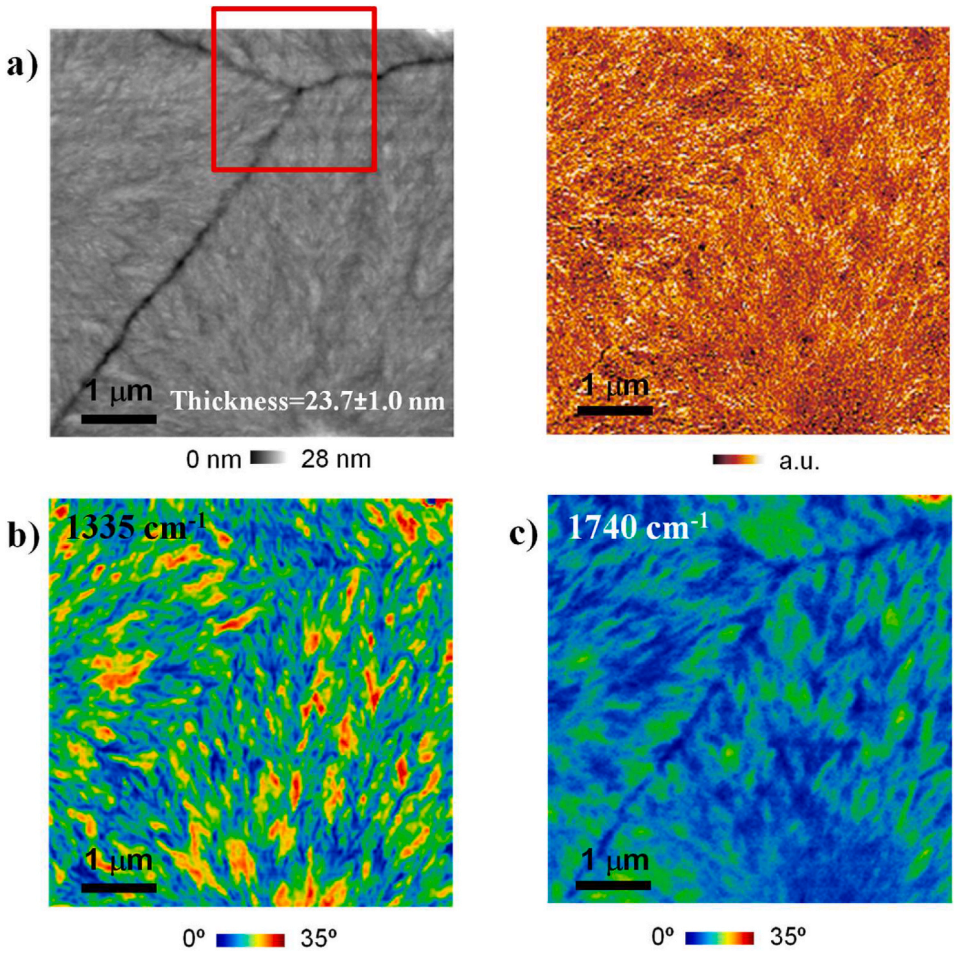

Fig. 5. **a)** AFM height image (left) and mechanical phase image (right) corresponding to sample 3-layer (PBS)_2 and near-field phase (i.e. absorption) images at **b)** 1335 cm^{-1} and **c)** 1740 cm^{-1}. The red square in Fig. 5a marks the region employed to carry out the analysis through nano-FTIR spectroscopy (shown in Fig. 6). (For interpretation of the references to colour in this figure legend, the reader is referred to the Web version of this article.)

macromolecules diffusion towards the crystal interface. Capillary flow occurring during the dip-coating process brings about a constant supply of polymer solution that contains the polymer that can crystallize [41]. In the case of the films under study here, as the evaporation rate is high (chloroform is a solvent with a high vapor pressure [42] and hence, capillary flow is high, the rapid polymer diffusion gives rise to complete spherulites/axialites due to a constant polymer supply. Still, the degree of crystallization of the PBS on the thin films under study is too low to be detected through GIWAXS experiments. Such low degree of crystallinity could be attributed to slow crystallization kinetics of PBS films casted from diluted chloroform solutions. PBS films under study here present thicknesses below 10 nm. As it has been reported in literature, polymer chains in ultrathin films usually crystallize slowly in proximity of interfaces [35].

3.3. Nanoscale chemical characterization by s-SNOM and nano-FTIR techniques

The technique of infrared near-field microscopy (IR s-SNOM) and nanospectroscopy (nano-FTIR) allows for infrared imaging and spectroscopy with nanoscale spatial resolution [43,44]. It has recently been employed to investigate submicrometer chemical distribution and crystallization of polymer blend films, as an example casted from PCL/PEG blends in THF [45]. In order to shed further light onto the chemical distribution of the three polymers, PBS, PCL and COPOL, onto the thin films prepared through sequential dip-coating, s-SNOM phase images and nano-FTIR phase spectra were recorded for samples corresponding to series II, 3-layer (PBS)_2 and 13_layer (PBS)_2. The probing depth of the nano-FTIR technique is up to 100 nm [46,47], which is related to the oscillation amplitude of the cantilever at a fixed point on the sample. Taking into account that the films under study present thicknesses in the range from 10 to 25 nm, the nano-FTIR results provide information about the whole sample. By using this technique, it is possible to obtain IR absorption spectra that correlate to bulk transmission infrared spectroscopy (e.g., FT-IR) as both techniques measure the amount of absorbed light [48].

As a first step, the main FTIR bands corresponding to the individual polymers were identified from nano-FTIR spectra of pristine thin films of PCL, PBS and COPOL. Fig. 4 shows representative spectra in the 1900-900 cm^{-1} range, in which it is possible to observe a large number of absorption bands and band overlaps (see the chemical structures in Figure S2 in the Supplementary Information). All three spectra show a C═O stretching band (at 1734 cm^{-1}) and a C–O–C stretching band (at 1174 cm^{-1} for PBS and COPOL and at 1190 cm^{-1} for PCL). However, the band at 1335 cm^{-1} band, assigned to the C–H asymmetric angular deformation, is strong in the PBS spectrum and absent in the PCL spectrum. In addition, the 1241 cm^{-1} band, assigned to the asymmetric stretching vibration of C–O–C group is very strong in the PCL spectrum and absent in the PBS spectrum. Additional FTIR bands located at 1295 and 1367 cm^{-1} are clearly visible in the FTIR spectrum corresponding to PCL which can be assigned to C–O and C–C stretching and C═O stretching in the crystalline phase, respectively [49,50]. PBS thin films under study present a low crystallinity as demonstrated through GIWAXS results, this was further demonstrated through analysis of the

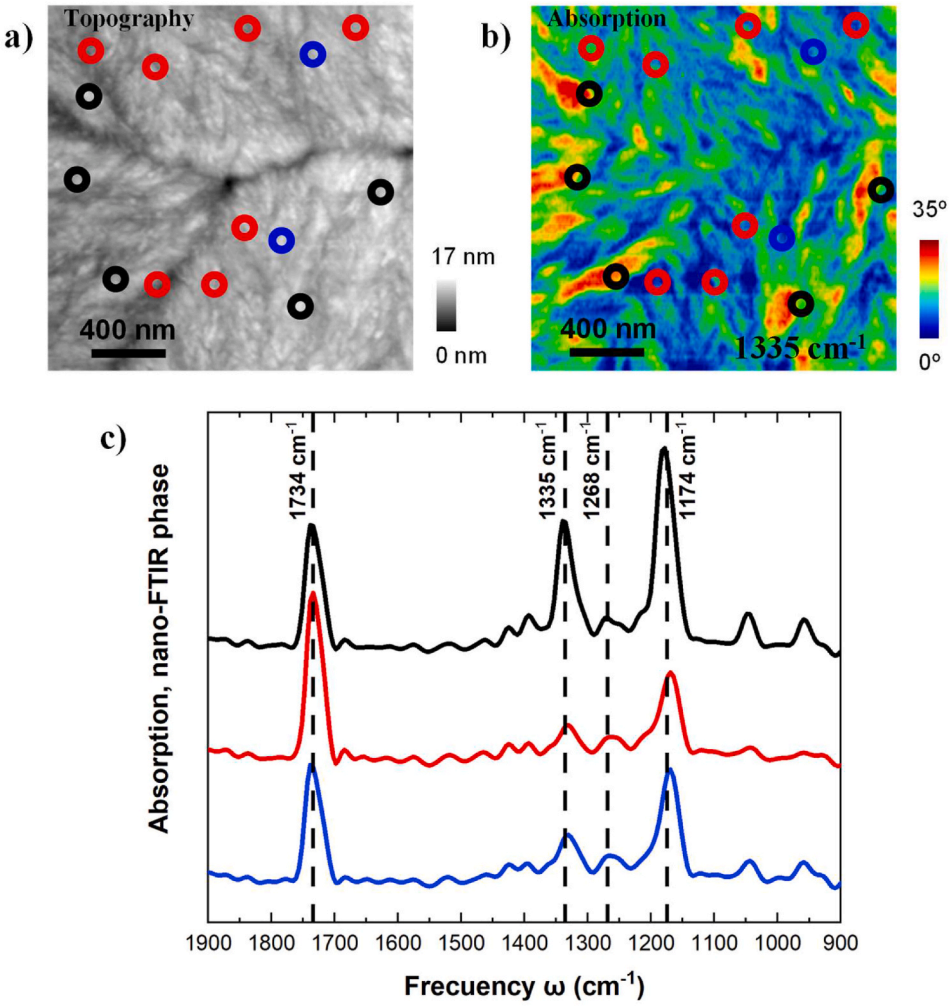

Fig. 6. **a)** AFM height image and **b)** absorption image at 1335 cm^{-1} corresponding to sample 3-layer (PBS)_2 and **c)** Nano-FTIR spectra obtained by averaging spectra recorded at the positions marked by corresponding blue, red and black colors in panel b. (For interpretation of the references to colour in this figure legend, the reader is referred to the Web version of this article.)

carbonyl region in the nano-FTIR spectra shown in the Supplementary Information, Figure S6. According to literature, the peak in the carbonyl region in FTIR can be deconvoluted to three absorption bands that can be assigned to the stretching mode of C═O groups in the crystalline phase (1714 cm^{-1}), in the rigid amorphous fraction (1720 cm^{-1}) and in the free amorphous fraction (1736 cm^{-1}) [51]. The nano-FTIR spectrum corresponding to PBS film showed a broad peak in the carbonyl region with the highest intensity located at 1730 cm^{-1}, which supports the low degree of crystallinity of the PBS film under study.

The absorption bands observed for COPOL are overlapped to those observed in neat PBS and neat PCL. However, the intensity ratio of the bands at 1335 cm^{-1} and 1241 cm^{-1} increases from ~2 in the spectra corresponding to COPOL to ~8 in the spectra corresponding to PBS, a result that reflects the presence of BS and CL sequences within the COPOL sample.

AFM height and mechanical phase images corresponding to sample 3-layer (PBS)_2 are shown in Fig. 5a. As can be observed, PBS crystalline superstructures (resembling spherulites or axialites) composed of PBS edge-on lamellar crystals growing from central nuclei are seen. The polygonal boundaries between these superstructures (produced by their impinging as they grow radially) are very clear in Fig. 5a. We assume that the lamellae observed are PBS, as PBS was the last material to be deposited in the film. This was confirmed by the strong contrast observed for the absorption images at 1335 cm^{-1} (Fig. 5b) and at 1740 cm-1 (Fig. 5c), which are characteristic infrared absorption bands for PBS (see Fig. 4). A compositional map corresponding to the sample 3-layer (PBS)_2 is shown in Figure S7 as supporting information. The image shows mainly blue areas where absorption is highest at 1740 cm^{-1} corresponding to the carbonyl region for the three polymers, PBS, PCL and COPOL and pink areas where absorption is highest at 1335 cm^{-1}, which has been identified as a characteristic infrared absorption band for PBS. From this image, it is not possible to ascertain the presence of PCL within the sample. Hence, to further investigate the polymers' chemical distribution, several nano-FTIR spectra were recorded at determined positions within the region marked by the red square in the AFM height image in Fig. 5a. An enlargement of this region is shown in Fig. 6a, and the corresponding absorption image at 1335 cm^{-1} (Fig. 6b). Several nano-FTIR spectra were recorded at different positions marked with red, black, and blue circles. The recorded individual nano-FTIR spectra show high quality and reproducibility (results not shown).

The black circles correspond to spots that showed high absorption at 1335 cm^{-1}, and the red circles correspond to positions that showed high absorption at 1740 cm^{-1} (see Fig. 5c). The blue circles correspond to positions with relatively low absorption at both IR frequencies. The corresponding average nano-FTIR spectra depicted in Fig. 6c show the characteristic C–O stretching band at 1734 cm^{-1} and the C–O–C stretching band at 1174 cm^{-1} that is overlapped for PBS, PCL, and COPOL. In addition, the three spectra show a band located at ~1335 cm^{-1} characteristic of PBS, as shown in Fig. 4. A broad band centered at ~1268 cm^{-1} is also observed for the three samples. The intensity ratios

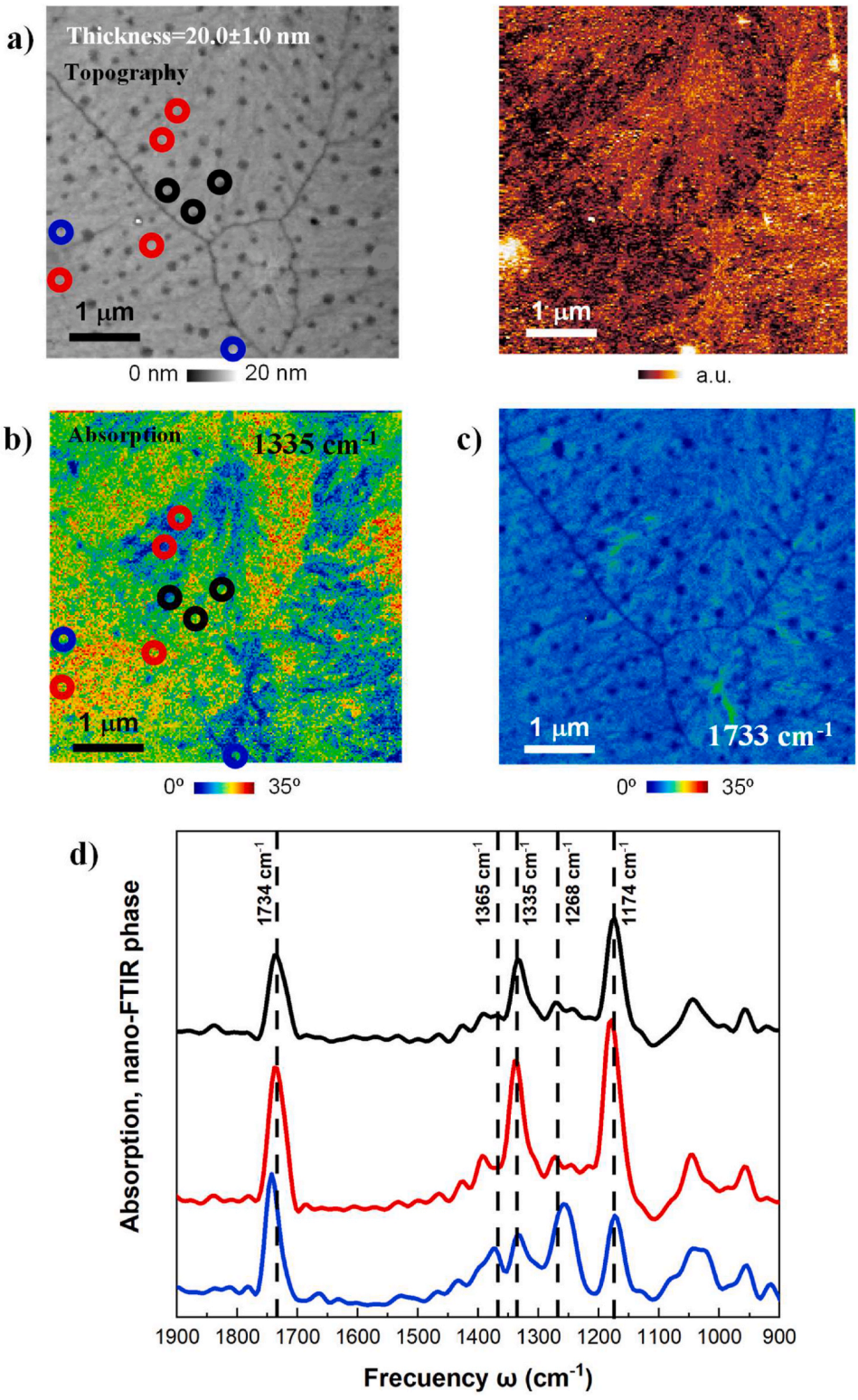

Fig. 7. a) AFM height image (left) and mechanical phase image (right) corresponding to sample 13-layer (PBS)_2, absorption images at **b)** 1335 cm^{-1} and **c)** 1733 cm^{-1}, and **d)** Nano-FTIR spectra obtained by averaging spectra recorded at the positions marked by corresponding black, red and blue colors in panel b. (For interpretation of the references to colour in this figure legend, the reader is referred to the Web version of this article.)

between the peak at 1268 cm^{-1} and the peak at 1335 cm^{-1} reveal differences in the infrared absorption in different positions of the 3-layer (PBS)_2 sample and thus in the chemical distribution within the sample. The I_{1335}/I_{1268} is ~5 for the average spectrum corresponding to positions marked with black, whereas I_{1335}/I_{1268} for the average spectra obtained from positions marked with blue and red colour decreases to ~2 for both cases, which reveals regions with higher relative content of CL sequences.

We now turn our attention to the results obtained for the 13-layer (PBS)_2 sample for which the total number of layers was increased

from 3 to 13. The morphology observed for this sample (Fig. 7a) is similar to the one described for sample 3-layer (PBS)_2, see Fig. 5a. That is, the number of dipping steps employed for the preparation of the sample does not seem to have an influence on the obtained morphology.

The presence of small holes on the 13-layer (PBS)_2 sample can be attributed to the rapid evaporation of chloroform during film preparation by dip-coating. As it is well known, when the solvent is rapidly evaporating, the solvent-rich films do not have enough time to level and heal surface roughness created by Marangoni instabilities. This effect and the resulting morphology could be tuned through the control of the evaporation rate during film preparation [42]. As in the case of the 3-layer (PBS)_2 sample, the absorption images taken at 1335 cm^{-1} and 1733 cm^{-1} (Fig. 7b and c, respectively) showed high contrast, which is more clearly observed for the image taken at 1335 cm^{-1}. This is consistent with the fact that the crystalline morphology can be attributed to the last deposited polymer, that is, to PBS.

The polymer distribution was further analyzed by recording several nano-FTIR spectra at different positions marked by coloured circles in the AFM height image (Fig. 7a, left) and the absoption image taken at 1335 cm^{-1} (Fig. 7b). Red circles correspond to locations outside the holes and black circles correspond to locations within the holes, as seen in the AFM topography image. Both red and black spectra shown in Fig. 7c fit nicely to the reference spectrum of PBS in agreement with the fact that the morphology observed is mostly due to PBS. In both cases, I_{1335}/I_{1268} is ~3, which indicates a similar chemical composition regarding BS/CL sequences. A close examination of the average nano-FTIR spectra obtained from regions marked with blue dots, which corresponds to positions with relatively low absorption at the IR frequency of 1335 cm^{-1}, allows to clearly distinguish a noticeable increase in the intensity of the band located at 1268 cm^{-1} with respect to the band located at 1335 cm^{-1}, which is much more evident in the case of the average spectrum obtained from regions marked with blue circles. For these regions, the band located at 1365 cm^{-1}, characteristic of PCL, is also clearly visible.

The results show that the increase in the number of deposited layers give rise to almost isolated PCL nanodomains within a matrix predominantly constituted of PBS. Thus it points to more segregation between BS and CL sequences for the 13-layer (PBS)_2 sample as compared to the 3-layer (PBS)_2 sample. The final morphology obtained for these thin films could be compared to that of an immiscible blend of PCL/PBS as previously reported in literature. This could be attributed to the fact that the repetitive dipping steps employed to prepare the sample leads to the deposition of mixed solutions of the three polymers due to the partial dissolution of the films during the dipping procedure.

4. Conclusions

In this study, sequential dip-coating of silicon substrates in chloroform solutions of PCL, PBS, and a poly (butylene succinate-*ran*-ε-caprolactone) (PBS-*ran*-PCL) copolymer has been employed to obtain thin polymer films with a varying number of layers (3 and 13). The thickness obtained for the films was, in all cases, in the range 10–25 nm regardless of the number of layers employed for their preparation, which points to partial dissolution of the films occurring during the process of preparation. The crystalline morphology observed corresponds to that of the last deposited polymer, as revealed by AFM microscopy. In the case of films for which the last deposited layer was PCL, diffraction peaks corresponding to the semicrystalline structure of PCL were detected by GIWAXS experiments. On the other hand, for films whose final layer was PBS, even if spherulitic/axialitic formation could be observed by AFM, no diffraction peaks were obtained in GIWAXS.

For films whose final layer was PBS, nano-FTIR spectroscopy provided the main evidences to determine the nanoscale organization of BS and CL sequences on 3-layer films and 13-layer films. The results showed that both samples present a heterogeneously mixed chemical composition with nanodomain regions of varying PBS and PCL content. However, in the case of 13-layer films, the analysis of the average spectra corresponding to different regions of the sample films revealed the presence of almost segregated PCL nanodomains within a PBS matrix. The results could be attributed to the fact that the partial dissolution of the film occurring during the sequential dipping steps might give rise to the deposition of a mixed solution of the three polymers resulting in a morphology that is reminiscent of that exhibited by immiscible blends.

Declaration of competing interest

The authors declare that they have no known competing financial interests or personal relationships that could have appeared to influence the work reported in this paper.

Acknowledgements

The authors acknowledge Pilar Posadas for AFM measurements and Iban Amenabar (External Services Department, CIC NanoGUNE San Sebastián) for nano-FTIR measurements. This study was supported by Spanish Ministry of Science, Innovation and Universities (MAT2017-83014-C2-1-P, MAT2017-83014-C2-2-P, PID2019-107514 GB-I00/AEI/10.13039/501100011033 and PID2019-106125 GB-I00/AEI/10.13039/501100011033). We also acknowledge funding by Basque Government through grant IT1309-19. The authors acknowledge beamtime access at ALBA BL11 via proposal 2018072905 and the assistance of JC Martinez during the measurements. We would also like to thank the financial support provided by the BIODEST project; this project has received funding from the European Union's Horizon 2020 research and innovation programme under the Marie Skłodowska-Curie grant agreement No. 778092. CO wants to acknowledge "Diputación Foral de Gipuzkoa" in the framework program "Fellows Gipuzkoa de Atracción y Retención de Talento". RH is member of the Interdisciplinary Platform for Sustainable Plastics towards a Circular Economy (SusPlast) from the Spanish National Research Council (CSIC).

Appendix A. Supplementary data

Supplementary data to this article can be found online at https://doi.org/10.1016/j.polymer.2021.123812.

Data availability statement

The raw/processed data required to reproduce these findings cannot be shared at this time due to technical or time limitations.

References

[1] M. Gigli, M. Fabbri, N. Lotti, R. Gamberini, B. Rimini, A. Munari, Poly(butylene succinate)-based polyesters for biomedical applications: a review, Eur. Polym. J. 75 (2016) 431–460, https://doi.org/10.1016/j.eurpolymj.2016.01.016.
[2] T.P. Gumede, A.S. Luyt, A.J. Müller, Review on PCL, PBS, AND PCL/PBS blends containing carbon nanotubes, Express Polym. Lett. 12 (2018) 505–529, https://doi.org/10.3144/expresspolymlett.2018.43.
[3] J. John, R. Mani, M. Bhattacharya, Evaluation of compatibility and properties of biodegradable polyester blends, J. Polym. Sci. Part A Polym. Chem. 40 (2002) 2003–2014, https://doi.org/10.1002/pola.10297.
[4] Z. Qiu, W. Yang, T. Ikehara, T. Nishi, Miscibility and crystallization behavior of biodegradable blends of two aliphatic polyesters. Poly(3-hydroxybutyrate-co-hydroxyvalerate) and poly(ε-caprolactone), Polymer 46 (2005) 11814–11819, https://doi.org/10.1016/j.polymer.2005.10.058.
[5] C. Ciulik, M. Safari, A. Martínez de Ilarduya, J.C. Morales-Huerta, A. Iturrospe, A. Arbe, A.J. Müller, S. Muñoz-Guerra, Poly(butylene succinate-ran-ε-caprolactone) copolyesters: enzymatic synthesis and crystalline isodimorphic character, Eur. Polym. J. 95 (2017) 795–808, https://doi.org/10.1016/j.eurpolymj.2017.05.002.
[6] R.A. Pérez-Camargo, I. Arandia, M. Safari, D. Cavallo, N. Lotti, M. Soccio, A. J. Müller, Crystallization of isodimorphic aliphatic random copolyesters: pseudo-eutectic behavior and double-crystalline materials, Eur. Polym. J. 101 (2018) 233–247, https://doi.org/10.1016/j.eurpolymj.2018.02.037.
[7] M. Safari, A. Mugica, M. Zubitur, A. Martínez de Ilarduya, S. Muñoz-Guerra, A. J. Müller, Controlling the isothermal crystallization of isodimorphic PBS-ran-PCL

random copolymers by varying composition and supercooling, Polymers 12 (2019) 17, https://doi.org/10.3390/polym12010017.
[8] L. Xue, J. Zhang, Y. Han, Phase separation induced ordered patterns in thin polymer blend films, Prog. Polym. Sci. 37 (2012) 564–594, https://doi.org/10.1016/j.progpolymsci.2011.09.001.
[9] M. Criado-Gonzalez, M. Fernandez-Gutierrez, J.S. Roman, C. Mijangos, R. Hernández, Local and controlled release of tamoxifen from multi (layer-by-layer) alginate/chitosan complex systems, Carbohydr. Polym. (2019), https://doi.org/10.1016/j.carbpol.2018.11.007.
[10] J.S. Gonzalez, C. Mijangos, R. Hernandez, Polysaccharide coating of gelatin gels for controlled BSA release, Polymers 11 (2019), https://doi.org/10.3390/polym11040702.
[11] M. Criado, E. Rebollar, A. Nogales, T.A. Ezquerra, F. Boulmedais, C. Mijangos, R. Hernández, Quantitative nanomechanical properties of multilayer films made of polysaccharides through spray assisted layer-by-layer assembly, Biomacromolecules 18 (2017), https://doi.org/10.1021/acs.biomac.6b01449.
[12] P. Lavalle, J.C. Voegel, D. Vautier, B. Senger, P. Schaaf, V. Ball, Dynamic aspects of films prepared by a sequential deposition of species: perspectives for smart and responsive materials, Adv. Mater. 23 (2011) 1191–1221, https://doi.org/10.1002/adma.201003309.
[13] K. Weng, L. Ye, L. Zhu, J. Xu, J. Zhou, X. Feng, G. Lu, S. Tan, F. Liu, Y. Sun, Optimized active layer morphology toward efficient and polymer batch insensitive organic solar cells, Nat. Commun. 11 (2020) 1–9, https://doi.org/10.1038/s41467-020-16621-x.
[14] H. Hwang, H. Lee, S. Shafian, W. Lee, J. Seok, K.Y. Ryu, D.Y. Ryu, K. Kim, Thermally stable bulk heterojunction prepared by sequential deposition of nanostructured polymer and fullerene, Polymers 9 (2017) 1–13, https://doi.org/10.3390/polym9090456.
[15] A. Larrañaga, E. Lizundia, A review on the thermomechanical properties and biodegradation behaviour of polyesters, Eur. Polym. J. 121 (2019) 109296, https://doi.org/10.1016/j.eurpolymj.2019.109296.
[16] G.E. Stein, T.S. Laws, R. Verduzco, Tailoring the attraction of polymers toward surfaces, Macromolecules 52 (2019) 4787–4802, https://doi.org/10.1021/acs.macromol.9b00492.
[17] J. Yang, Y. Liang, W. Shi, H.S. Lee, C.C. Han, Effects of surface wetting induced segregation on crystallization behaviors of melt-miscible poly(l-lactide)-block-poly (ethylene glycol) copolymer thin film, Polymer 54 (2013) 3974–3981, https://doi.org/10.1016/j.polymer.2013.05.032.
[18] M. Ma, Z. He, J. Yang, Q. Wang, F. Chen, K. Wang, Q. Zhang, H. Deng, Q. Fu, Vertical phase separation and liquid-liquid dewetting of thin PS/PCL blend films during spin coating, Langmuir 27 (2011) 1056–1063, https://doi.org/10.1021/la104003p.
[19] M. Ma, F. Chen, K. Wang, Q. Zhang, H. Deng, Z. Li, Q. Fu, Anisotropic dewetting holes with instability fronts in ultrathin films of polystyrene/poly(∈-caprolactone) blend, Macromolecules 45 (2012) 4932–4937, https://doi.org/10.1021/ma3000779.
[20] S.S. Roland, D. Gaspard, R.E. Prud'homme, C.G. Bazuin, Morphology Evolution in Slowly Dip-Coated Supramolecular PS-B-P4vp Thin Films, 2012, https://doi.org/10.1021/ma3007398.
[21] S.S. Roland, C. Pellerin, C.G. Bazuin, R.E. Prud'homme, Evolution of Small Molecule Content and Morphology with Dip-Coating Rate in Supramolecular PS−P4VP Thin Films, 2012, https://doi.org/10.1021/ma301383v.
[22] A. Vital, M. Vayer, T. Tillocher, R. Dussart, M. Boufnichel, C. Sinturel, Morphology control in thin films of PS:PLA homopolymer blends by dip-coating deposition, Appl. Surf. Sci. 393 (2017) 127–133, https://doi.org/10.1016/j.apsusc.2016.09.151.
[23] D. Grosso, How to exploit the full potential of the dip-coating process to better control film formation, J. Mater. Chem. 21 (2011) 17033–17038, https://doi.org/10.1039/c1jm12837j.
[24] J.R. Smith, D.A. Lamprou, Polymer coatings for biomedical applications: a review, Trans. Inst. Met. Finish. 92 (2014) 9–19, https://doi.org/10.1179/0020296713Z.000000000157.
[25] A.I. Visan, G. Popescu-Pelin, O. Gherasim, A. Mihailescu, M. Socol, I. Zgura, M. Chiritoiu, L.E. Sima, F. Antohe, L. Ivan, D.M. Vranceanu, C.M. Cotrut, R. Cristescu, G. Socol, Long-term Evaluation of Dip-Coated PCL-Blend-PEG Coatings in Simulated Conditions, 2020, https://doi.org/10.3390/polym12030717. Polymers (Basel).
[26] M. Safari, A. Martínez De Ilarduya, A. Mugica, M. Zubitur, S. Muñoz-Guerra, A. J. Müller, Tuning the thermal properties and morphology of isodimorphic poly [(butylene succinate)- ran-(ε-caprolactone)] copolyesters by changing composition, molecular weight, and thermal history, Macromolecules 51 (2018) 9589–9601, https://doi.org/10.1021/acs.macromol.8b01742.
[27] Q. Liu, X.M. Zhou, Preparation of poly(butylene succinate)/poly(ε-caprolactone) blends compatibilized with poly(butylene succinate-co-ε-caprolactone) copolymer, J. Macromol. Sci. Part A Pure Appl. Chem. 52 (2015) 625–629, https://doi.org/10.1080/10601325.2015.1050634.
[28] A.P. Hammersley, FIT2D: a multi-purpose data reduction, analysis and visualization program, J. Appl. Crystallogr. 49 (2016) 646–652, https://doi.org/10.1107/S1600576716000455.
[29] A.A. Govyadinov, I. Amenabar, F. Huth, P. Scott Carney, R. Hillenbrand, Quantitative measurement of local infrared absorption and dielectric function with tip-enhanced near-field microscopy, J. Phys. Chem. Lett. 4 (2013) 1526–1531, https://doi.org/10.1021/jz400453r.
[30] I. Amenabar, S. Poly, M. Goikoetxea, W. Nuansing, P. Lasch, R. Hillenbrand, Hyperspectral infrared nanoimaging of organic samples based on Fourier transform infrared nanospectroscopy, Nat. Commun. 8 (2017), https://doi.org/10.1038/ncomms14402.
[31] I. Amenabar, S. Poly, W. Nuansing, E.H. Hubrich, A.A. Govyadinov, F. Huth, R. Krutokhvostov, L. Zhang, M. Knez, J. Heberle, A.M. Bittner, R. Hillenbrand, Structural analysis and mapping of individual protein complexes by infrared nanospectroscopy, Nat. Commun. 4 (2013) 1–9, https://doi.org/10.1038/ncomms3890.
[32] C. Qiao, J. Zhao, S. Jiang, X. Jl, A.N. Lijia, B. Jiang, Crystalline morphology evolution in PCL thin films, J. Polym. Sci., Part B: Polym. Phys. 43 (2005) 1303–1309, https://doi.org/10.1002/polb.20422.
[33] M. Ma, Z. He, J. Yang, F. Chen, K. Wang, Q. Zhang, H. Deng, Q. Fu, Effect of film thickness on morphological evolution in dewetting and crystallization of polystyrene/poly(ε-caprolactone) blend films, Langmuir 27 (2011) 13072–13081, https://doi.org/10.1021/la2036289.
[34] D. Maillard, R.E. Prud'homme, Crystallization of ultrathin films of polylactides: from chain chirality to lamella curvature and twisting, Macromolecules 41 (2008) 1705–1712, https://doi.org/10.1021/ma071306u.
[35] J. Spièce, D.E. Martínez-Tong, M. Sferrazza, A. Nogales, S. Napolitano, Are polymers glassier upon confinement? Soft Matter 11 (2015) 6179–6186, https://doi.org/10.1039/c5sm01229e.
[36] J.J. Hernández, D.R. Rueda, M.C. García-Gutiérrez, A. Nogales, T.A. Ezquerra, M. Soccio, N. Lotti, A. Munari, Structure and morphology of thin films of linear aliphatic polyesters prepared by spin-coating, Langmuir 26 (2010) 10731–10737, https://doi.org/10.1021/la100959j.
[37] I.-K. Yang, C. Yun Liu, Real-time SAXS and WAXS study of the multiple melting behavior of poly(e-caprolactone), J. Polym. Sci., Part B: Polym. Phys. 48 (2010) 1777–1785, https://doi.org/10.1002/polb.22035.
[38] M. Safari, J. Maiz, G. Shi, D. Juanes, G. Liu, D. Wang, C. Mijangos, ángel Alegría, A. J. Müller, How confinement affects the nucleation, crystallization, and dielectric relaxation of poly(butylene succinate) and poly(butylene adipate) infiltrated within nanoporous alumina templates, Langmuir 35 (2019) 15168–15179, https://doi.org/10.1021/acs.langmuir.9b02215.
[39] T.P. Gumede, A.S. Luyt, R.A. Pérez-Camargo, A. Tercjak, A.J. Müller, Morphology, nucleation, and isothermal crystallization kinetics of Poly(Butylene Succinate) mixed with a polycarbonate/MWCNT masterbatch, Polymers 10 (2018) 1–22, https://doi.org/10.3390/polym10040424.
[40] A.B. Meyer, PhD Thesis, University of Hamburg, 1998..
[41] M. Vayer, A. Pineau, F. Warmont, M. Roulet, C. Sinturel, Constrained crystallization of poly(L-lactic acid) in thin films prepared by dip-coating, Eur. Polym. J. 101 (2018) 332–340, https://doi.org/10.1016/j.eurpolymj.2018.03.006.
[42] K.E. Strawhecker, S.K. Kumar, J.F. Douglas, A. Karim, The critical role of solvent evaporation on the roughness of spin-cast polymer films, Macromolecules 34 (2001) 4669–4672, https://doi.org/10.1021/ma001440d.
[43] F. Huth, A. Govyadinov, S. Amarie, W. Nuansing, F. Keilmann, R. Hillenbrand, Nano-FTIR absorption spectroscopy of molecular fingerprints at 20 nm spatial resolution, Nano Lett. 12 (2012) 3973–3978, https://doi.org/10.1021/nl301159v.
[44] D. Richards, A. Zayats, Nano-Optics and Near-Field Optical Microscopy, Artech House, Boston/London, 2008.
[45] P. Nguyen Tri, R.E. Prud'Homme, Crystallization and segregation behavior at the submicrometer scale of PCL/PEG blends, Macromolecules 51 (2018) 7266–7273, https://doi.org/10.1021/acs.macromol.8b01503.
[46] L. Mester, A.A. Govyadinov, S. Chen, M. Goikoetxea, R. Hillenbrand, Subsurface chemical nanoidentification by nano-FTIR spectroscopy, Nat. Commun. 11 (2020) 1–10, https://doi.org/10.1038/s41467-020-17034-6.
[47] T. Taubner, F. Keilmann, R. Hillenbrand, Nanoscale-resolved subsurface imaging by scattering-type near-field optical microscopy, Opt Express 13 (2005) 8893, https://doi.org/10.1364/opex.13.008893.
[48] A. Dazzi, C.B. Prater, AFM-IR: technology and applications in nanoscale infrared spectroscopy and chemical imaging, Chem. Rev. 117 (2017) 5146–5173, https://doi.org/10.1021/acs.chemrev.6b00448.
[49] A.K. Monrreal-Rodríguez, J.A. Garibay-Alvarado, C.L. Vargas-Requena, S.Y. Reyes-López, In vitro evaluation of poly-ε-caprolactone-hydroxypatite-alumina electrospun fibers on the fibroblast's proliferation, Results Mater 6 (2020) 100091, https://doi.org/10.1016/j.rinma.2020.100091.
[50] T. Elzein, M. Nasser-Eddine, C. Delaite, S. Bistac, P. Dumas, FTIR study of polycaprolactone chain organization at interfaces, J. Colloid Interface Sci. 273 (2004) 381–387, https://doi.org/10.1016/j.jcis.2004.02.001.
[51] S.F. Yao, X.T. Chen, H.M. Ye, Investigation of structure and crystallization behavior of poly(butylene succinate) by fourier transform infrared spectroscopy, J. Phys. Chem. B 121 (2017) 9476–9485, https://doi.org/10.1021/acs.jpcb.7b07954.